

OPEN

Co-occurrence of marine and atmospheric heatwaves with drought conditions and fire activity in the Mediterranean region

Raquel Santos¹✉, Ana Russo^{2,3} & Célia M. Gouveia^{1,2}

Climate change has become a major concern in the twenty-first century, leading to the amplification of extreme events and, consequently, to severe impacts on society, economy and ecosystems. Heatwave conditions in particular, often coupled with extended periods of dryness, have an important contribution in exacerbating rural fires. Here, we propose to analyse the co-occurring interplay between atmospheric heatwaves and droughts in southern Europe, and marine heatwaves in the East Atlantic and the Mediterranean Sea, between 2001 and 2022, highlighting their linkage to wildfires, on both an individual and compound approach. Positive correlations between air and sea temperatures and negative correlations between air temperature and precipitation values were found. Our analysis reveals that severe wildfires are mostly associated with reduced precipitation and/or elevated air temperatures during the summer season, alongside heightened sea surface temperatures. Marine hot (drier) conditions are prevalent for months in which burned areas remain below (above) the 80th percentile. Months marked by higher fire activity are predominantly associated with extreme climatic conditions, showcasing a substantial occurrence of compound events. This study highlights the potential of considering both land-based atmospheric and marine conditions when exploring compound extremes, crucial for mitigating climatic disasters. Moreover, it highlights the role played by compound extreme events in fire management strategies, particularly considering the present context of climate change and the increasing frequency and severity of extreme events threatening ecosystem stability.

Climate change is a prominent concern of the twenty-first century, leading to the occurrence of extreme weather events, among which heatwaves stand out as they have increased in frequency, duration, and intensity¹. Characterized by prolonged and consecutive periods of anomalously warm temperatures², heatwaves can occur both in the ocean–marine heatwaves (MHWs)^{2,3}, or in the atmosphere–atmospheric heatwaves (AHWs)⁴. Heatwaves in the Mediterranean region have become increasingly prevalent, with significant escalations observed in their characteristics over the recent decades across all of its basins^{4–6}. These events have significant repercussions on the ecosystems, human health and increased death rates^{7,8}, fire incidence occurrence^{9–11} and ecological disruptions, triggering terrestrial and marine species^{12–14}.

Climate change has also been manifesting through the persistent occurrence of droughts¹⁵, which have substantial effects on human mortality¹⁶, vegetation dynamics^{17–21}, agricultural production^{22–24}, fire coverage^{25,26}, water supply and quality²⁷, and the reliability of hydroelectricity generation²⁸. An increased frequency and severity of droughts is expected, particularly in the Mediterranean region, under future climate change scenarios, emphasizing the critical requirement for advanced drought assessment methodologies and the necessity for interdisciplinary research to develop resilient strategies against the multifaceted impacts of droughts²⁹. The Mediterranean basin, which has been repeatedly highlighted as a climate change hot-spot^{30,31}, has experienced some remarkable impacts (e.g., wildfires) that have inflicted widespread destruction upon natural ecosystems

¹Instituto Português do Mar e da Atmosfera (IPMA), 1749-077 Lisboa, Portugal. ²Instituto Dom Luiz, Faculdade de Ciências, Universidade de Lisboa, 1749-016 Lisboa, Portugal. ³CEF - Forest Research Centre, Associate Laboratory TERRA, School of Agriculture, University of Lisbon, Lisboa, Portugal. ✉email: raquel.santos@ipma.pt

and human resources^{25,32–35}. This region is facing a growing threat of more frequent wildfires, the most extreme of which occur during co-occurring drought and heatwave episodes. Under the most pessimistic scenario (RCP8.5), the frequency of wildfires driven by simultaneous warm and dry conditions is expected to increase by 30% by the end of the century (2071–2100)¹⁰.

The combination of climate drivers and/or hazards—not necessarily extreme—leading to significant social and environmental impact, constitutes a "compound event"³⁶. These episodes can occur simultaneously in space and/or time, or in close succession (time-lagged)^{37,38}. Given their complexity and their consequences, that often exceed those observed when each condition acts independently, they have been receiving increasing attention from the scientific community^{21,24,34–39} and the media. Research projections suggest their future intensification^{40–42}, posing significant challenges for adaptation strategies. As examples, compound events involving extreme winds and precipitation will increase in frequency, especially in regions with higher emissions scenarios⁴³. Compound heatwaves and droughts are also expected to become more common across all emission scenarios globally⁴³, which can have a toll on other aspects as heatwaves interact with other hazards. Namely, heatwaves and ozone pollution form one of the most impactful compound events across the world⁴⁴. In the marine environment, the co-occurrence of MHWs and ocean acidity extremes has a vital role, often leading to larger impacts on marine ecosystems⁴⁵. The importance of compound events' occurrence has been analysed also by⁴⁶, highlighting the impact of the intensity and duration of marine heatwaves on low chlorophyll events, characterizing their compound nature and the associated role of climate variability. Moreover, understanding the response of phytoplankton to extreme climatic events (e.g., MHWs, droughts) is crucial and has been a focus of study in various regions of the world^{46–48}, as it is a fundamental component of the marine food chain. The projected impacts of climate change indicate an intensification of marine compound events which are expected to have increasing pressure on marine organisms and ecosystems exposed to multiple biogeochemical changes in the coming decades^{49,50}.

One of the most significant impacts concerning the compound effect of hot and dry conditions relates to the occurrence of wildfires, largely driven by the synergy of increased temperatures, decreased soil moisture, and low humidity levels which, together with the fuel accumulation and dryness, enhance the likelihood of fire ignition^{10,21,26,34,35}. Namely,³⁵ explored the conditions that led to the massive rural fires that took place in Portugal in 2017, pointing to a conjugation of factors: (1) a prolonged drought leading to preconditioned cumulative hydric stress of vegetation, (2) unusual meteorological conditions caused by the passage of hurricane Ophelia off the Coast of Portugal, and (3) negligent human-induced ignitions from agricultural practices. The compound nature of droughts and hot extremes has been associated with disastrous wildfires across multiple regions, such as in Australia⁵¹, California⁵², North Africa⁵³, Brazil²⁶ and other regions of Europe^{10,34,35}.

Although numerous studies have been conducted on the combined influence of AHWs and droughts on fire occurrence^{33–35,54}, the combined analysis of MHWs and AHWs and its linkage with the occurrence of other events remains still underexplored. It has been shown that, under the influence of human activity, not only atmospheric but also marine heatwaves are more likely to occur^{3,55} and future projections indicate that these events are expected to continue increasing, as global warming proceeds^{14,56–58}. A few studies have investigated a connection between sea surface temperatures (SST) and atmospheric temperatures during heatwaves, which may be attributed to shared primary drivers, but may also arise from the complex atmosphere–ocean interactions^{58,59}. Research studies carried out by^{60,61}, determined that the co-occurrence of terrestrial and coastal MHWs is significantly frequent over the eastern Mediterranean Basin and coastal regions of Australia, respectively. Reference⁶² also revealed the existence of a significant coupling between coastal MHWs and increased air temperatures and humidity over adjacent cities around the world during the summer season, particularly pronounced at higher latitudes. During the exceptional 2003 European AHWs, the Mediterranean Sea surface temperatures (SSTs) were abnormally high. AHWs over Europe resulted in increased rates of air-sea heat fluxes in the Mediterranean Sea which, together with reduced wind speeds, led to the warming of surface waters^{11,63–65}. Certain studies also highlight the significance of these high SSTs in the persistence of the tropospheric anticyclone over the western Mediterranean, thereby intensifying the AHWs¹¹. The role of atmospheric processes in driving the co-occurrence of extreme events in the atmosphere and the ocean is also highlighted in⁵⁹. The authors explored the mechanisms involving local changes in the air-ocean heat fluxes associated with atmospheric blocking in inducing severe drought conditions and triggering the development of MHWs in the adjacent ocean during the summer of 2013/2014 in eastern South America.

Even though the nexus between extreme events namely between drought–heatwaves, drought–fires, heatwaves–fires and heatwaves–droughts–fires has been deeply explored, the synergy between MHWs, AHWs and droughts and their association with fire activity still have not been critically examined over Mediterranean Europe. Considering the importance of compound events and the synergistic effects they have on exacerbating extreme fire outbreaks, the primary objective of this study is to analyse the occurrence of heatwaves (both marine and atmospheric) as well as drought episodes and their single and compound association with the occurrence of rural fires in the Mediterranean region over the past decades. The highly innovative and crucial evaluation of the synergies between these contributing factors, will significantly improve the understanding of the mechanisms underlying fire behaviour, which is critical for developing preventive strategies aimed at reducing the devastating effects of wildfires.

Data and methodology

Study area and datasets

The study area is defined by the domain ranging from 30° N to 52° N and from 20° W to 38° E. We mainly focus on three areas, shown in the panels of Fig. 1, as our objective is to concentrate on regions particularly susceptible to fire risk^{66,67} and the adjacent marine areas. The figure shows the land cover classification types within the region of study, derived from the European Space Agency Climate Change Initiative (ESA CCI) Land Cover (LC) project,

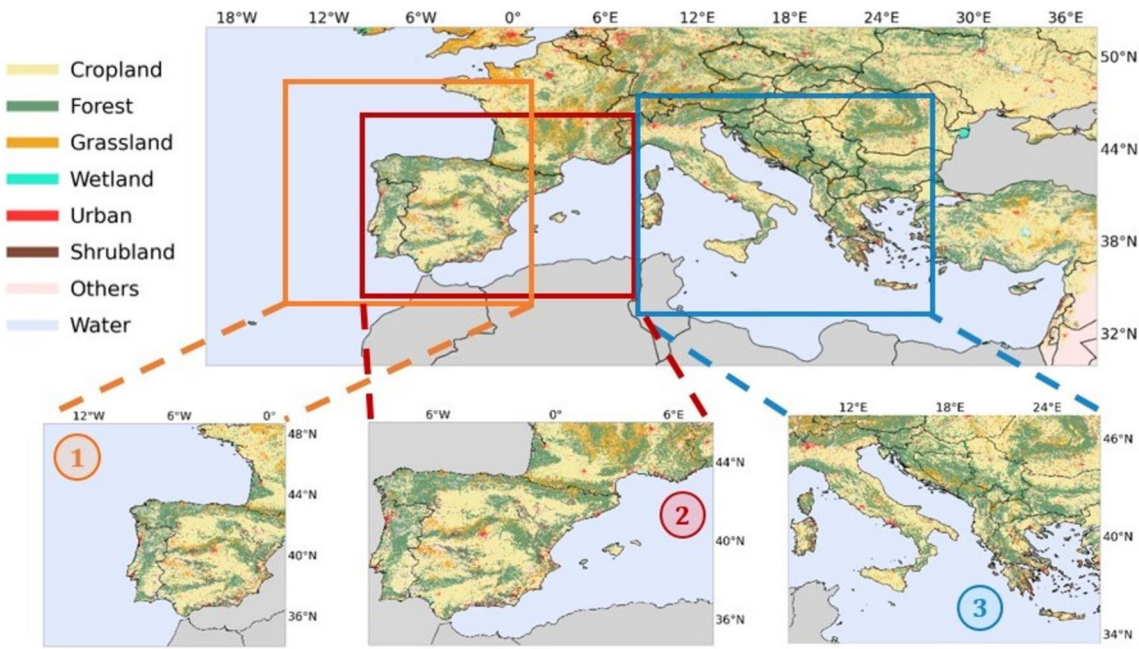


Figure 1. Domain of study. Based on ESA CCI LC data, land cover classes are shown based on information for the year 2020. Three subregions were chosen: Region 1) centered on Iberia and considering the Northeast Atlantic region and excluding the Mediterranean Sea, Region 2) centered on Iberia and Mediterranean France, considering the western Mediterranean Sea, Region 3) centered on Italy and the Peloponnese, considering the eastern Mediterranean Sea. Areas shown in gray are masked. This image was produced using the environment Spyder IDE 5.1.5 with Python 3.9.12, available at <https://www.spyder-ide.org/>.

which is made accessible through the Copernicus Climate Change Service (C3S) Climate Data Store (CDS)⁶⁸. The dataset with a horizontal resolution of 300 m provides yearly data that covers the period from 1992 to 2020. The LC classification is divided into 22 global classes (level 1) and 37 regional classes (level 2). In this work, LC classes were extracted for the years 2001–2020 and grouped into six main categories: cropland (corresponding to ESA CCI LC numbers from 10 to 30), grassland (110,130), urban (190), forest (50–100, 160, 170), wetland (180), shrubland (120–122), water (210) and others (40, 140–143, 200–202, 220).

To analyse AHWs and MHWs, 2-m air temperature (T2m) and sea surface temperature (SST) were respectively used. The data was extracted from the ERA5 reanalysis, provided by the European Centre for Medium-Range Weather Forecast (ECMWF)⁶⁹. Total precipitation (P) data from ERA-5, given by the sum of large-scale and convective precipitation, is also extracted to assess drought conditions in the region. ERA-5 is the fifth generation of atmospheric reanalysis produced by ECMWF, which offers several atmospheric, ocean and land variables estimated through the combination of model data with observations, with a 0.25° regular spatial resolution⁷⁰. Hourly T2m, SST and total precipitation data were derived for the period spanning from 1979 to 2022 within the defined study region.

Burned area (BA) data was acquired from the MCD64A1 Version 6 Burned Area Product⁷¹ from NASA's Moderate Imaging Spectroradiometer (MODIS) sensor aboard the Terra and Aqua satellite platforms. This dataset provides monthly values with a 500-m spatial resolution, offering estimates of the ordinal day of burn for all pixels identified as burned. Its algorithm results from the combination of daily surface reflectance imagery with daily active fire data to map BAs. When compared to previous versions, MDC64A1v006 exhibits less sensitivity to the presence of cloud contamination. Furthermore, it detects smaller fires more precisely and provides reduced uncertainty in the estimation of the date of the burn⁷². Data on BA was extracted from 2001 to 2022, since no data retrieved by this sensor is available prior to this period and was accessed through the Application for Extracting and Exploring Analysis Ready Samples⁷³.

In this work, a simplified classification approach is used to categorize pixels into two distinct groups, as our sole requirement pertains to determining whether a pixel has undergone burning or not^{21,38}. All pixels that are identified as burned, regardless of the specific ordinal day of the burn, are assigned a value of 1. Conversely, all other pixels, including those that are unburned, unmapped due to data limitations, and those over water, are assigned a value of 0.

The calculation of BAs in hectares is performed using the Haversine formula, which is widely used to compute distances between two points on the surface of a sphere. Here, the Haversine formula is applied to calculate distances on Earth by considering the latitude and longitude coordinates of two points. Although the result is approximate as the formula assumes the Earth to be a perfect sphere, this is still a valuable tool to compute distances on the Earth's surface⁷⁴.

Values of BA were normalized by dividing by the corresponding areas of each region to analyze the evolution of fire-affected areas. Such normalization enables a consistent comparison of burned areas across different regions, and facilitates a more rigorous analysis, as was utilized in prior works^{75,76}.

This work is primarily concerned about fires that are mostly related to adverse climatic factors, namely heatwaves and droughts. These fires are not actively controlled by agricultural management practices. To distinguish such fires from cropland fires, which are primarily associated with intentional use for agricultural purposes⁷⁷, the LC yearly classification from the ESA CCI LC dataset is used. This data, which originally has a spatial resolution of 300 m, was resampled, using the nearest neighbour and majority rule interpolation techniques, to match the 500-m resolution of the BA data. The LC dataset only covers the period from 1992 until 2020. To address this limitation, the data from 2020 is also used for the years 2021 and 2022, allowing the identification and exclusion of cropland areas from the study.

Marine and atmospheric heatwaves

One of the problems when analysing heatwaves statistically is related to the fact that a universal definition is non-existent. Previous studies have employed different definitions and indices to study the occurrence of heatwaves^{78–80}. Therefore, the lack of a universally accepted definition has often resulted in ambiguity and inconsistency in the analysis. In this study, we follow the approach proposed by² since it provides a consistent terminology, definition and metrics which enable meaningful comparisons between different heatwave events across different locations and time periods. This definition was firstly applied for AHWs and then minor adjustments were introduced so it could have a broader definition to account for the longer time scales of ocean variability compared to the atmosphere. We apply this methodology, which has been widely used in numerous studies^{3,12,57}, to define both AHWs and MHWs to uphold consistency and facilitate the interpretation of comparisons of heatwave characteristics in both cases. Considering this, we define heatwaves as periods with daily temperatures above the 90th percentile for at least 5 consecutive days². The climatological mean and the 90th percentile are calculated at each grid cell for each calendar day. The reference period over which the events are defined covers all years from 1979 to 2022, following the minimum recommendation of 30 years proposed by the WMO⁸¹. If any interval of two days or less between heatwaves occurs, a continuous single event is considered. As ERA5 data offers an hourly resolution, daily aggregations were performed to determine the maximum daily temperatures, by identifying the highest temperature recorded over the 24-h period for each day⁷⁹. In this study, AHWs are only analysed over land pixels, and the oceanic region is solely characterized by MHWs.

Once identified, heatwaves can be characterized by some properties, as described in⁸². The duration of the event is defined as the period over which daily temperatures exceed the defined threshold, and the intensity of the event is quantified by measuring the difference between the observed temperature and the corresponding climatological value. Within a certain event, the maximum intensity is the highest temperature deviation relative to the climatology, while the mean intensity represents the average temperature anomaly during the heatwave. The intensity composite index (ICI) serves as a composite measure that summarizes the heatwave properties mentioned above and is computed through the following formula:

$$ICI = \sum_{i=1}^n \sum_{d=1}^{d_i} \Delta T(i, d) \quad (1)$$

where $i = 1, \dots, n$ is the number of heatwave events, d is the duration of the i -th event, and $\Delta T(i, d)$ measures the intensity of the i -th event on its d -th day. This means that temperature anomalies are successively accumulated whenever a heatwave occurs over a specific period of time (units: °C-days). In this study, ICI is calculated monthly and yearly, to capture heatwave conditions on both a monthly and annual scale. These properties were applied to both AHWs and MHWs.

Drought conditions

Drought events can be characterized through the computation of a panoply of indicators. The use of indicators relies on three main principles: (1) Simplicity: Drought indices are relatively easy to calculate and interpret, making them a valuable tool; (2) Comprehensiveness: Drought indices can take into account a variety of factors that contribute to drought, such as precipitation, temperature, and evapotranspiration. This allows them to provide a more holistic assessment of drought conditions than any single factor alone; (3) Flexibility: Drought indices can be adapted to specific regions and time scales, making them a versatile tool for drought assessment. Two of the most commonly used indices are the SPI (Standardized Precipitation Index) and SPEI (Standardized Precipitation-Evapotranspiration Index), which allow the identification of drought or wet events as well as the characterization of their duration, intensity, and magnitude, and have been applied in multiple studies^{75,83,84}. The SPI was proposed by⁸⁵ as a drought monitoring index that relies solely on precipitation data and is widely used due to its simplicity. It is nowadays the index recommended by the WMO⁸⁶, not without caveats⁸⁷. SPI has the advantage of being a multiscalar index, being comparable in time and space, allowing to monitor drought response with respect to different ecosystems. However, it is not able to account for the influence of temperature, which has been rising throughout the world in the last decades. On the other hand, SPEI, developed by⁸⁷, not only considers precipitation but also evapotranspiration (PET) data in its computation and it is also a multiscalar index, allowing for more effective detection of the effects of climate change on drought conditions while accounting for the influence of temperature variability and extremes. For this reason, the analysis in this study relies on the SPEI.

The computation of SPEI was made using the period between 1979 and 2022 as the reference period, only considering the land pixels. Monthly accumulated precipitation was calculated, and evapotranspiration (ET0) was also determined by applying the Hargreaves equation, which relies on maximum and minimum temperature

records⁸⁸. The Hargreaves method, with its simplicity and low data requirements, emerges as an alternative that allows for the estimation of PET reliably when compared to the more complex FAO Penman–Monteith equation^{89,90}. The difference between the precipitation and the ET0 provides a measure of water excess or deficit^{85,86}. A log-logistic probability distribution was fitted to model the water deficit with a rectangular adjustment, resulting in a normal distribution with a mean of zero and a standard deviation of one, where positive values indicate wetter conditions and negative values imply drier conditions.

The index was calculated monthly and has the advantage of analysing droughts at different temporal scales, capturing the accumulated drought conditions over shorter or longer periods. The 12-month time scale is usually able to identify drought events on an annual perspective. The 3-month SPEI reflects soil water conditions of short to medium duration and allows for seasonal drought recognition⁸⁷. In this study, SPEI was computed at timescales of 3 and 12 months (respectively, SPEI-3 and SPEI-12 hereafter), to explore drought conditions on both a seasonal and annual scale.

Areas affected by drought conditions can be identified based on probability classes. According to⁹¹, moderate droughts correspond to a probability of occurrence of 0.201 (approximately the 20th percentile of the SPI series, -0.84), while severe and extreme droughts correspond to a probability of 0.10 (-1.28) and 0.05 (-1.65), respectively. In this work, these thresholds are considered based on the SPEI.

Interannual evaluation and coincidence analysis

To investigate the interannual changes in heatwave conditions during the whole period, yearly spatial averaging is performed for all of the heatwave properties considering the full region of study. Yearly spatial averages of SPEI-12 in December are also computed, as well as the percentage of pixels in moderate and severe levels of dryness, capturing the interannual drought conditions in the domain of study. The time evolution trends of heatwave properties and drought conditions are then tested for statistical significance using a Wald test with a t-distribution and a significance level of 0.05.

The statistical relationship between temperature and precipitation patterns was evaluated for two different periods: 1979–2000 and 2001–2022, through the computation of two probability density functions using a bivariate Gaussian distribution, which we assume is suitable for seasonal values of precipitation and temperature⁹². The bivariate distribution was computed for different pairs of variables: T2m-P, SST-P and T2m-SST. For the cases of T2m and SST, daily maximum values were considered, whereas for P, daily accumulated values were taken into account. These pairs of variables were averaged over the different regions of interest, considering an extended summer season (May to October). Our focus on the summer season is motivated by the high fire activity in Mediterranean countries, driven by reduced precipitation and exceptionally high temperatures that create conditions conducive to the ignition and rapid spread of fires in the Mediterranean region^{25,93,94}. We expanded the analysis to include late spring and early autumn months (May and October) to account for an identified tendency for longer fire seasons⁹⁴ and ensure that important wildfire events are considered (e.g., wildfires in October of 2017, Portugal)³⁵. The Pearson correlation coefficient between each pair is calculated and its statistical significance is assessed, testing using the Monte Carlo method at a significance level of 0.05. Univariate Gaussian distributions are also used to compute probability density functions of each variable for the two periods, to analyse how T2m, SST and P average anomaly patterns individually changed over time in the different regions.

To investigate the long-term relationship between areas affected by wildfires and the occurrence of hot and dry conditions, the spatial means of the yearly atmospheric ICI and SPEI-12 in December were analysed over the burned pixels annually, spanning all regions under investigation and all months of the year, between 2001 and 2022. BA's data's resolution differs from the ICI and SPEI data's resolution. Therefore, we computed the values of ICI and SPEI for each burned pixel by averaging the values from its four nearest points in ERA5's resolution. As marine ICI does not overlap geographically with the other variables, the ICI in the ocean was averaged yearly for the different marine areas of study to provide a clearer understanding of the phenomenon under investigation and how it may be associated with the occurrence of the other events.

Adopting a similar methodology to understand the synergy between short-term extreme events and fire extent, the spatial-averaged atmospheric ICI and SPEI-3 over burned pixels and spatial-averaged marine ICI in the surrounding areas were calculated in each region for every month between 2001 and 2022. The 80th percentile of the monthly atmospheric and marine ICI and the 20th percentile of the monthly SPEI-3 were used to identify the 20% warmest and driest months in the considered period, examined solely in the months where BA's were identified, allowing us to isolate the months that experienced the most intense conditions. The months characterized by such warmth and dryness were explored, considering both individual and compound occurrences. The decision to use the 80th percentile threshold was guided by a comprehensive sensitivity analysis. This threshold provided an optimal result by capturing the most relevant extreme conditions. This choice allowed us to focus on the most impactful months, ensuring a robust analysis of the synergy between extreme climatic events and fire extent. Furthermore, in this evaluation, we distinguished between months when the overall burned area equalled or surpassed the 80th percentile and those that fell below this threshold. This differentiation provides valuable insights into the factors linked to the occurrence of notably extensive fires compared to those of lesser dimensions.

Results

Temporal evolution of heatwave and drought conditions

Both marine and atmospheric yearly averages of ICI, number of events, mean duration and mean intensity of heatwaves demonstrate a statistically significant increasing trend (Fig. 2). Variations in the yearly frequency of events are consistent when considering both curves (Fig. 2a), with a significant increase of ~ 3.7 events in the atmosphere and ~ 4.2 events in the sea over the entire period. Except for the initial years, the mean duration of

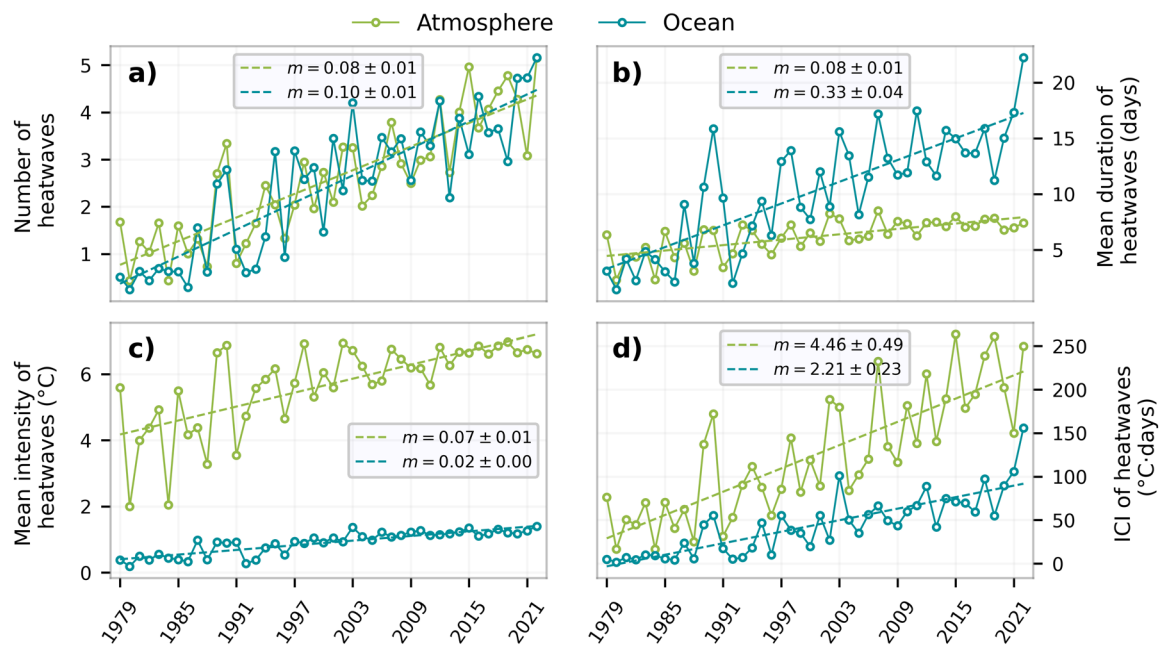


Figure 2. Temporal evolution of heatwave properties, between 1979 and 2022: (a) number of heatwaves, (b) mean duration of heatwaves (days), (c) mean intensity of heatwaves (°C) and (d) ICI (°C-days). Blue curves represent MHW, being area-averaged over the ocean pixels, while green curves denote AHW, area-averaged over the land pixels. This analysis considers the full region of study. The dashed lines indicate significant linear trends detected by the Wald Test with a t-distribution, considering a 0.05 significance level. Slope (m) values indicate trends over time, whose units vary as follows: (a) events/year, (b) days/year (c) °C/year, (d) °C-days/year.

events is always higher in the ocean, which also shows more emphasized yearly values and a steeper upward trend (yearly increase of 0.33 days for MHWs and 0.08 days for AHWs) (Fig. 2b). Mean durations in the ocean also show higher levels of variability in comparison with the atmosphere. The mean intensity of heatwaves reveals greater values and variability over the atmosphere, showing an increase of ~ 3 °C in anomalies between 1979 and 2022 (Fig. 2c). In the ocean, the average intensities exhibit reduced variability, showing an increase of ~ 1 °C over the whole period. The ICI of heatwaves (Fig. 2d) exhibits an upward trend considering both AHWs and MHWs due to its dependence on the other three heatwave properties. Higher values and a more accentuated trend are evidenced in the atmosphere, aligning with the patterns observed in mean intensity. Notably, the majority of years exhibit consistent behaviour when comparing the ICI values in the atmosphere and the ocean. In the latter half of the 1980s, specific years experienced significantly high ICI values, particularly in the atmosphere, due to heightened heatwave frequency (Fig. 2a) and mean intensity (Fig. 2c). However, in the most recent years, the situation has intensified considerably, due to a combination of heightened intensity, frequency, and duration of events, surpassing previous levels. The atmospheric ICI in 2015 was particularly intense in parts of central Europe and the southeastern Iberian Peninsula, followed by an increased ICI concentrated in Eastern Europe in 2019 and in western Europe in 2022. The Mediterranean Sea contributed to the highest ICI (cumulative intensity) values in 2003, 2018, and 2022 (Fig. S1, Supplementary Material).

The temporal evolution of drought conditions is shown in Fig. 3. The observed fluctuation in the temporal evolution of drought conditions (Fig. 3) depicted in both panels illustrates a pronounced variability in drought levels throughout the study period. In the current century, there is a higher prevalence of years characterized by dry conditions, with only 36% of years exhibiting positive SPEI levels. Among these years, 2010 stands out as the most humid one, while 2011, 2015 and 2022 reveal to be the driest ones. In contrast, the twentieth century witnessed 73% of years with positive SPEI levels. The most significant exceptions are the years 1989 and 1990, which were notably hot as revealed by heatwave characteristics (Fig. 2), and also strongly affected by drought conditions (Fig. 3). Moderate droughts exhibit greater frequency and have experienced a more significant increase over the years compared to severe droughts. Positive and statistically significant trends are evident in the below panel for both moderate (rate of 0.54% of area per year) and severe droughts (rate of 0.35% of area per year), indicating a consistent rise from 1979 to 2022. The years affected by the highest percentage of drought conditions (2003, 2015, 2022), whether moderate or severe, were affected across much of the European continent (Fig. S2, Supplementary Material).

Long-term changes in the correlation between temperature and precipitation

The relationship between mean T2m, SST and P during the extended summer season for 1979–2000 and 2001–2022 for all regions of interest is analysed through the computation of bivariate Gaussian probability distribution functions (Fig. 4). Additionally, univariate probability distribution functions are depicted to visually demonstrate the temporal evolution of temperature and precipitation anomalies individually.

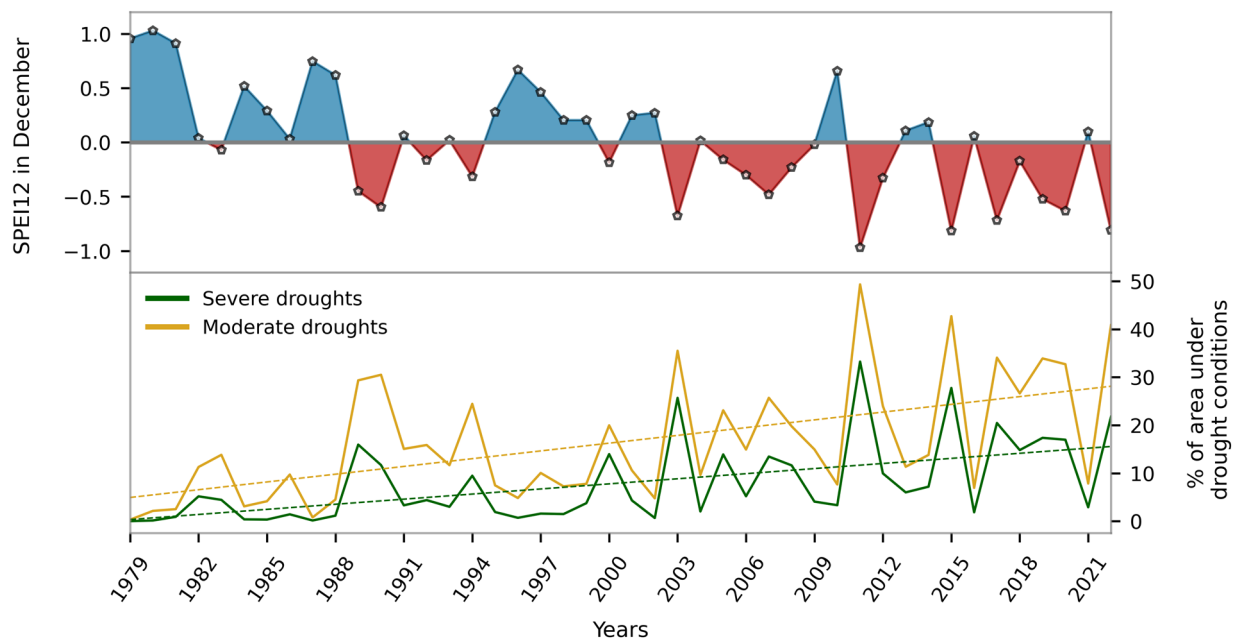


Figure 3. Temporal evolution of drought conditions. In the upper panel are displayed the spatial-averaged values of the 12-month SPEI for December over land between 1979 and 2022, and the below panel shows the percentage of area under the occurrence of severe droughts (green curve) and moderate droughts (yellow curve), using the definition by⁸¹. This analysis considers the full region of study. The dashed lines indicate significant linear trends detected by the Wald Test with a t-distribution, considering a 0.05 significance level.

In all cases, both T2m and SST have drastically changed when comparing both periods, exhibiting an abrupt shift towards higher values in the second period. When examining the mean values of accumulated precipitation, this transition exhibits a minor shift showing a contrast between eastern and western regions. In regions 1 and 2, over Western Europe, univariate PDF's reveal drier conditions in 2001–2022, while in region 3, there is a slight increase in the mean accumulated precipitation values in this period, uncovering the presence of wetter conditions.

In all regions, correlations between T2m-P show to be negative and significant in both periods, highlighting the inverse relationship between these variables. This correlation is higher in 2001–2022 than in the former period, in the full region (from -0.5 to -0.56) and region 2 (from -0.66 to -0.70). The correlation between SST-P shows to be negative and minimal in the first period. In the second period, the correlation rises considering the full region, region 1 and region 2. However, in neither of the periods these correlations are statistically significant. Regarding the analysis of T2m-SST, there is a strong and significant positive correlation between both variables in both periods, emphasizing the clear increase and connection between both variables over the analyzed periods. The correlation coefficients reveal to be higher in the second period for all analysed regions. Specifically, for the full region and region 1, the coefficients increase to 0.74, while for regions 2 and 3, they rise to 0.86 (Table S1, Supplementary Material).

Fire activity and its relationship with temperature and precipitation patterns

Fire occurrence has varied considerably throughout the years and along the different regions of Europe, as revealed by Fig. 5. Given the lack of BA data before 2001, only the period 2001–2022 will be analysed in the following sections. When analysing the entire Mediterranean area, 2017 was the most severe year, with a record of more than 900.000 hectares burned from May to October, followed by 2003 and 2007, which burned ~ 690.000 hectares in the same period. In Eastern Europe (region 3), the year 2007 was the most exceptional of all, having burned a total of ~ 500.000 hectares in the extended summer months. In Western Europe, regions 1 and 2 demonstrate similar patterns concerning the extent of BA's, owing to their significant geographical overlap, although region 1 typically exhibits a higher incidence of burning, as demonstrated by its higher normalized values. The years of 2017, 2003, 2005 and 2022 stand out as the most impactful in terms of normalized BA's in the extended summer for these regions.

Regarding Fig. 6, when considering the whole region, notable instances of severe burned area extent, including the years 2017, 2003, 2012, and 2022, were linked to reduced precipitation and elevated air and sea temperatures, when compared to the average values, during the summer season. The year 2003 experienced the driest conditions, while 2022 observed the highest sea and air temperatures since the beginning of the century. Despite its exceptional BA value, the summer of 2007 exhibited relatively less dryness and warmth compared to the average conditions.

In regions 1 and 2, as already stated, 2017, 2003, 2005 and 2022 stood out as notable when considering the extent of BA's. As expected, both regions exhibit analogous patterns. Some of the most severe years in terms of BA's are situated within the sector of the plots characterized by higher T2m and SST and lower precipitation

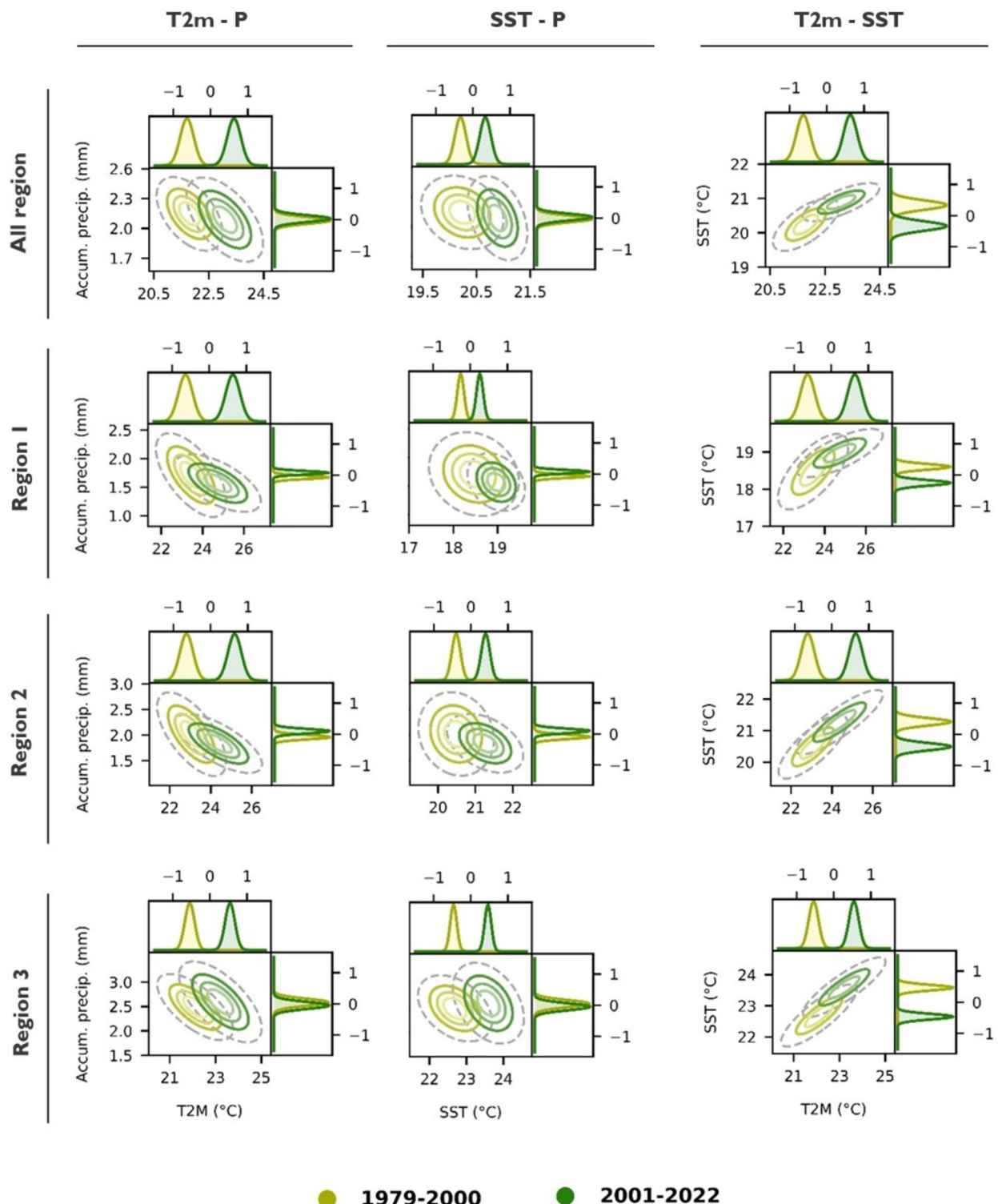


Figure 4. Correlation between temperature and precipitation patterns. The centre panel of each plot show the bivariate Gaussian probability distribution functions of extended summer mean temperatures (SST and T2m, °C) and accumulated precipitation (mm), and the lateral panels of each plot show the univariate probability distribution functions of the corresponding average anomalies (in the units of the corresponding absolute values). These functions are calculated for the period 1979–2000 in yellow, and 2001–2022 in green, and are averaged over all the regions of interest. The dashed gray ellipses represent the 95% level of the Gaussian probability distributions. Pearson correlation coefficients were computed using the Monte Carlo test, considering a significance level of 0.05.

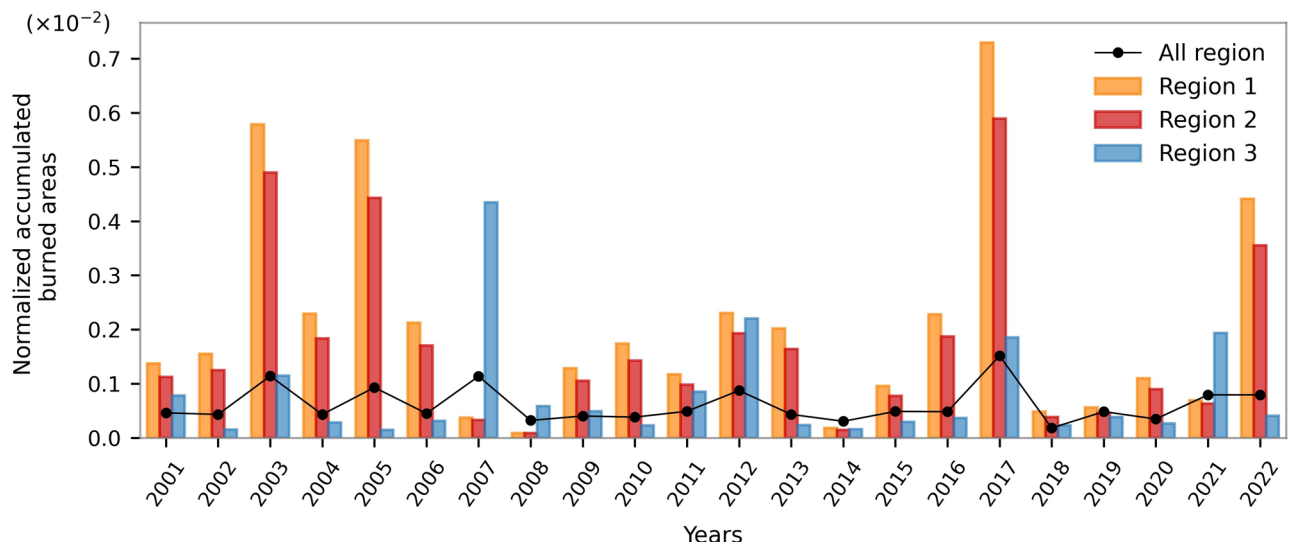


Figure 5. Temporal evolution of fire activity. Yearly normalized burned areas throughout the extended summers for region 1 (orange bars), region 2 (red bars), region 3 (blue bars) and for the overall study region (black curve). Normalized burned areas are obtained by dividing the BA's in hectares by the total land hectares in each of the regions.

levels. The year 2017 reveals to be the driest of those that burned the most, while 2022 the hottest one. The year 2003 was marked by high air temperatures, although it was wetter than average. In region 1, all the significant highlighted years in terms of BA's exhibit Atlantic's SST values higher than average. In region 2, a comparable pattern is observed, except that 2005 does not manifest very high SST values in the Mediterranean Sea. A noteworthy distinction between the two regions is evident: SST values in the Mediterranean (region 2) tend to be consistently higher than those in the Atlantic Ocean (region 1).

In the eastern Mediterranean (region 3), the most extensive burned year, 2007, exhibited SSTs, T2Ms and precipitation levels relatively close to the average. Conversely, the second most impactful year, 2012, was notably characterized by a very hot and dry summer, with SSTs in the Mediterranean also exceeding the average. The summers of 2017 and 2021 can also be emphasized by their accumulated burned hectares, associated to very dry conditions and temperatures close to the average. The years with less extreme burned area extents (2002, 2005, and 2014) correspond to the least extreme SSTs, T2Ms, and precipitation values.

Overall, it is seen that summers with the most extensive burned areas are commonly associated with dry and/or hot conditions. These conditions extend beyond air temperatures to encompass elevated sea temperatures as well.

Annual heatwave and drought conditions over burned regions

To specifically analyse heatwave and drought indices over burned pixels annually, Fig. 7 shows the yearly spatial means of atmospheric ICI and SPEI-12 for December, examined solely over the burned pixels in all study regions, between 2001 and 2022, considering all months of the year. The annual marine ICI is also averaged over the adjacent marine areas in each of these regions.

When examining the full region, it is observed that all the years exhibiting an average marine ICI below the 50th percentile also tend to be associated with less dry or less warm (or both) conditions over BA's (compared to the established threshold that delineates extreme years), except for 2017. Conversely, some of the years falling below the 50th percentile of marine ICI, mainly 2003, did not exhibit very extreme values for atmospheric ICI and SPEI-12. The years 2007, 2012, 2014, 2015, 2017, 2018, 2020, and 2022 all registered marine ICI values surpassing the 50th percentile while simultaneously recording extreme atmospheric ICI and SPEI-12 values, revealing that the conditions over the BA's were considerably hot and arid, and concurrently, the ocean temperatures were also substantially elevated during those years. Although not recording a high annual marine ICI value, 2017 stood out as the most extreme year in terms of atmospheric ICI and SPEI-12, recording the highest annual burned areas as well (Fig. S3, Supplementary Material). Meanwhile, 2022 emerged as the most severe year regarding the annual marine ICI.

Considering the partial overlap of land areas between regions 1 and 2, the spatial averaged values of atmospheric ICI and SPEI-12 exhibit similarity. The significant contrast between these regions relates to the higher marine ICI values registered in the Mediterranean Sea (region 2) when compared to the Atlantic Ocean (region 1). In both regions, 2017 stands out as the warmest and driest year across the BA's. This year was also the one that burned the most (Fig. S3, Supplementary Material). The years 2015 and 2022 also experienced very high air temperatures over burned pixels, although the SPEI-12 value remains below the 20% most extreme cases for 2022. In all these three cases, temperatures over the Mediterranean Sea were above the 80th percentile threshold. The Mediterranean Sea consistently exhibited higher temperatures compared to the Atlantic Ocean in nearly 80% of

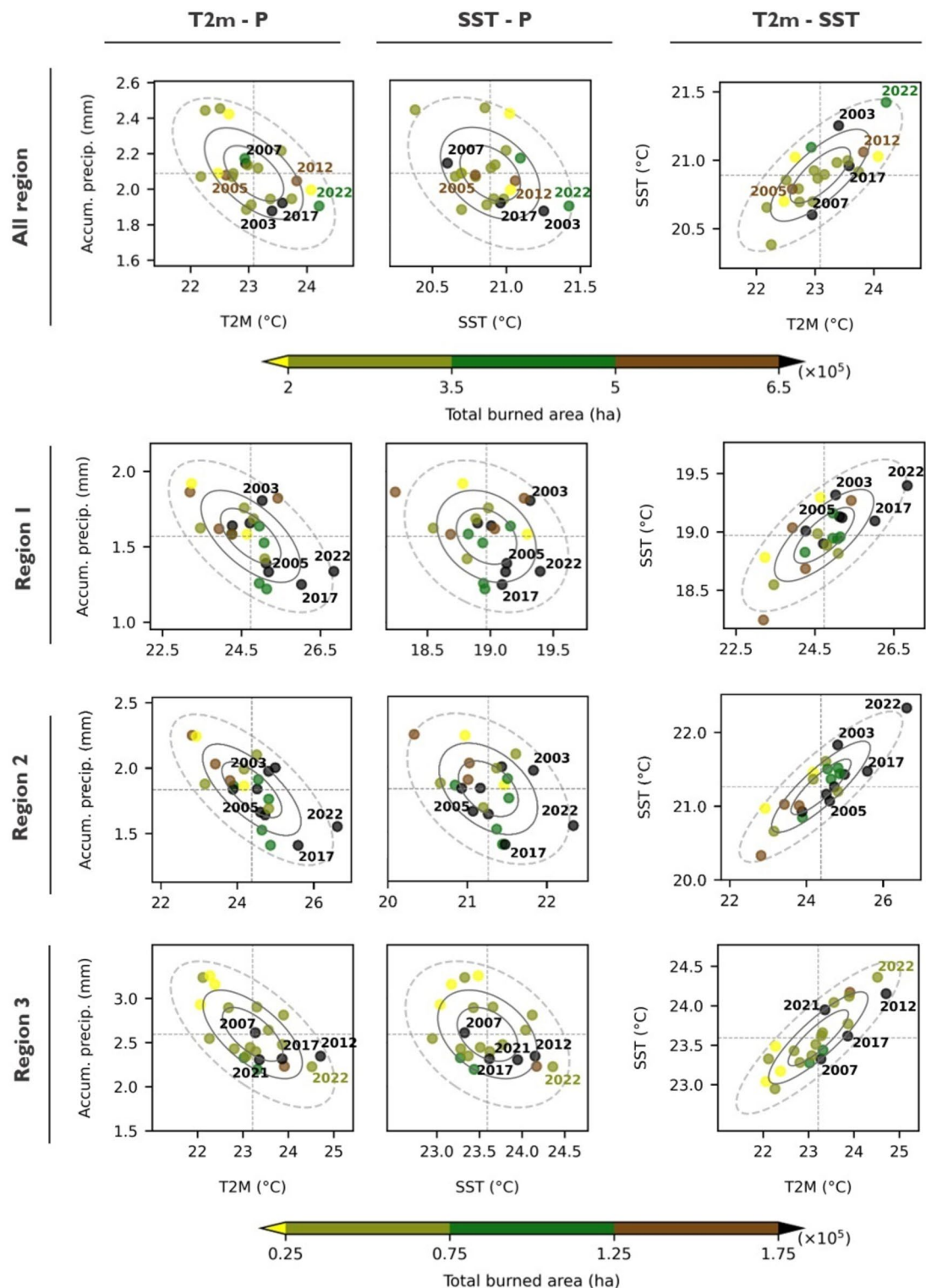


Figure 6. Temperature and precipitation patterns and its relationship with the burned area extent. Average values of daily accumulated precipitation and daily maximum temperatures (SST and T2m) for each year, calculated for the extended summer, are represented by the scatter points, and the summer accumulated burned area for each year is represented by the different colors. The bivariate Gaussian probability distributions of all pairs of variables for the period 2001–2022 are represented by the gray ellipses. The dashed gray ellipses represent the 95% level of the Gaussian probability distributions. Horizontal and vertical dashed lines correspond, respectively, to precipitation and temperature values averaged over all years of study.

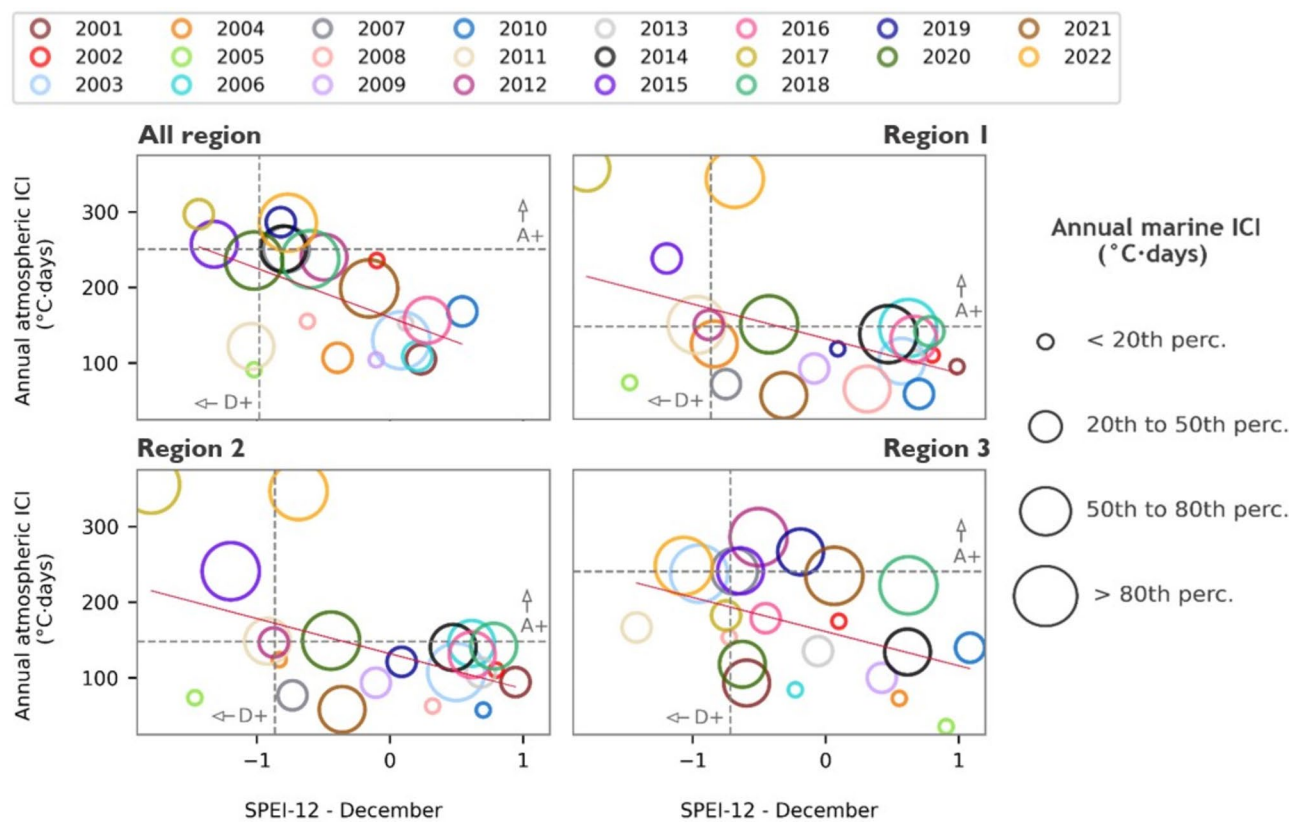


Figure 7. Annual heatwave and drought conditions over burned regions. Spatial averages of the annual accumulated atmospheric ICI ($^{\circ}\text{C}\text{-days}$) and SPEI-12 for December over burned pixels, regarding each of the study regions. In each region, the annual marine ICI ($^{\circ}\text{C}\text{-days}$) is averaged over the corresponding marine areas and represented through the size of the scatter points, which represent different percentiles. The different scatter colours describe different years from 2001 to 2022. Horizontal and vertical dashed lines separate the 20% most extreme cases regarding the atmospheric ICI (A+) and SPEI-12 values (D+), obtained through the computation of the 80th and 20th percentile, respectively.

the years. All years registering marine ICI values below the 20th percentile tend to be associated with less dry and warm conditions in comparison to the threshold, except for 2012 for both regions and 2015 for region 1.

In region 3, years for which the average marine ICI surpasses the 80th percentile closely correspond to or exceed the 80th percentile of atmospheric ICI over burned pixels. Notable examples of such extreme years include 2003, 2012, and 2022. The years 2003 and 2022 also revealed to be drier than the threshold. Conversely, years with average marine ICI below the 50th percentile are shown to coincide with less hot and dry conditions over BA's (except for 2011, which revealed to be very dry). In this case, the year 2012, which shows the second highest burned areas (Fig S3, Supplementary Material), revealed the most extreme atmospheric heatwave conditions and the second most extreme marine heatwave conditions in the surrounding sea.

In all the examined cases, the red line illustrates a negative and significant trend between atmospheric ICI and December SPEI-12 values for burned pixels. This means that years characterized by stronger heatwave conditions tend to also experience drier conditions, and vice-versa. This underscores the negative correlation previously observed in Fig. 5 between precipitation and air temperatures.

Monthly heatwave and drought conditions over burned regions

Heatwave and drought conditions over BA's are examined on a monthly scale. The distribution of the months affected by the 20% driest and warmest (both in the ocean and the atmosphere) conditions was identified (Fig. 8). This approach provides insights into the occurrence of short-term climatic extreme events in the areas affected by wildfires. Simultaneously, an analysis is conducted to identify months characterized by more or less extensive wildfires, using the 80th percentile of the monthly total burned area. It is apparent that August consistently records the highest frequency of years with total burned area exceeding the 80th percentile threshold across all analysed regions, followed by June and July. The summer of 2022 showed to be particularly extreme in all regions, mainly regarding region 2, where June, July and August revealed to be under the occurrence of all climatic hazards. The presence of the driest and warmest months is evidenced during the latter period (2012–2022), when compared to 2001–2011. This observation is coupled with the finding that the incidence of fires associated with non-extreme climatic events decreases during this period.

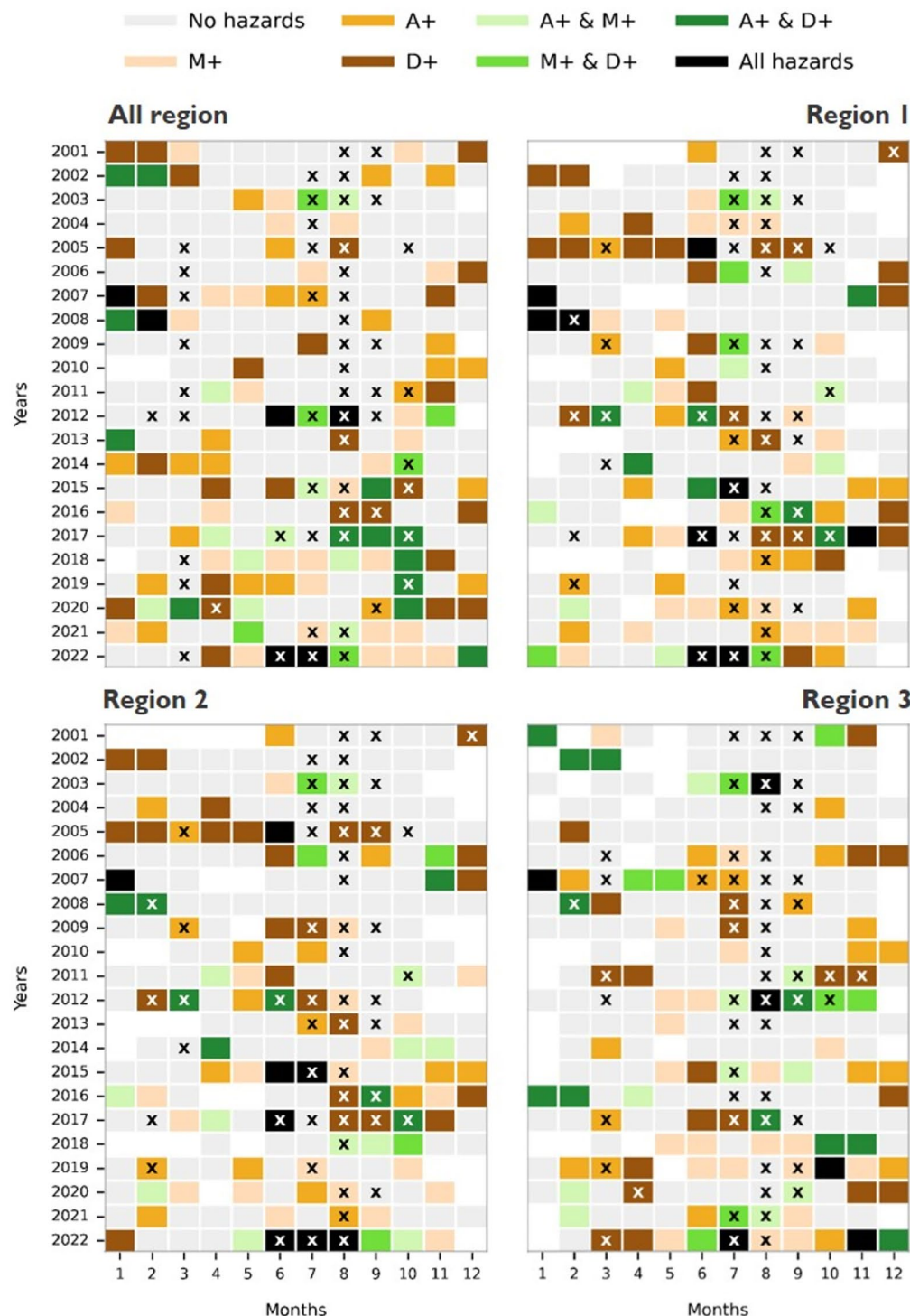


Figure 8. Monthly occurrences of single and compound hazards from 2001 to 2022. The 20% warmest and driest months are identified, and represented by colors, which delineate the occurrence of individual or combined climatic conditions. Specifically, "A+ and M+" denote a month with atmospheric and marine ICI equal to exceeding the 80th percentile, "D+" marks a month when the SPEI-3 value equals or falls below the 20th percentile. Meanwhile, months marked with an "X" indicate those where the burned area equals or exceeds the 80th percentile. Months that did not record any burned pixels are filled in blank.

Figure 9 showcases the portion of months associated with the occurrence of the 20% warmest (atmospheric: A+, and marine: M+ and driest conditions (D+), considering both individual and compound occurrences, in

each region of study. This analysis is conducted separately in months where the total burned area either exceeded or fell below the 80th percentile threshold. Regarding the left column, which refers to months that did not reach the 80th percentile threshold of accumulated burned area, consistency is shown across all regions of study. The occurrence of these fires is predominantly associated with occurrences of M+ episodes, constituting approximately 9–14% of all months. Subsequently, D+ episodes are observed and following are A+ events, except for region 3, where A+ episodes are more recurrent than D+ events. The remaining combinations of hazards exhibit lower occurrence rates. Notably, approximately 60% of all months with BA's below the 80th percentile did not experience any of these extreme hazards. Examining months where the total burned area exceeded the 80th percentile threshold, observed in the right column of Fig. 9, D+ events emerge as the most prevalent hazard across all regions of study, occurring in 11–19% of cases. Subsequent rates vary based on individual regions. Overall, these months, marked by more extensive fires, demonstrate a stronger connection with the occurrence of extreme hazards in comparison to months with less extensive fires. Specifically, in regions 1, 2 and 3, over 50% of the months are linked to any type of extreme climatic events. Furthermore, the occurrence of compound hazards is generally more frequent when considering months with a broader extension of BA's, covering more

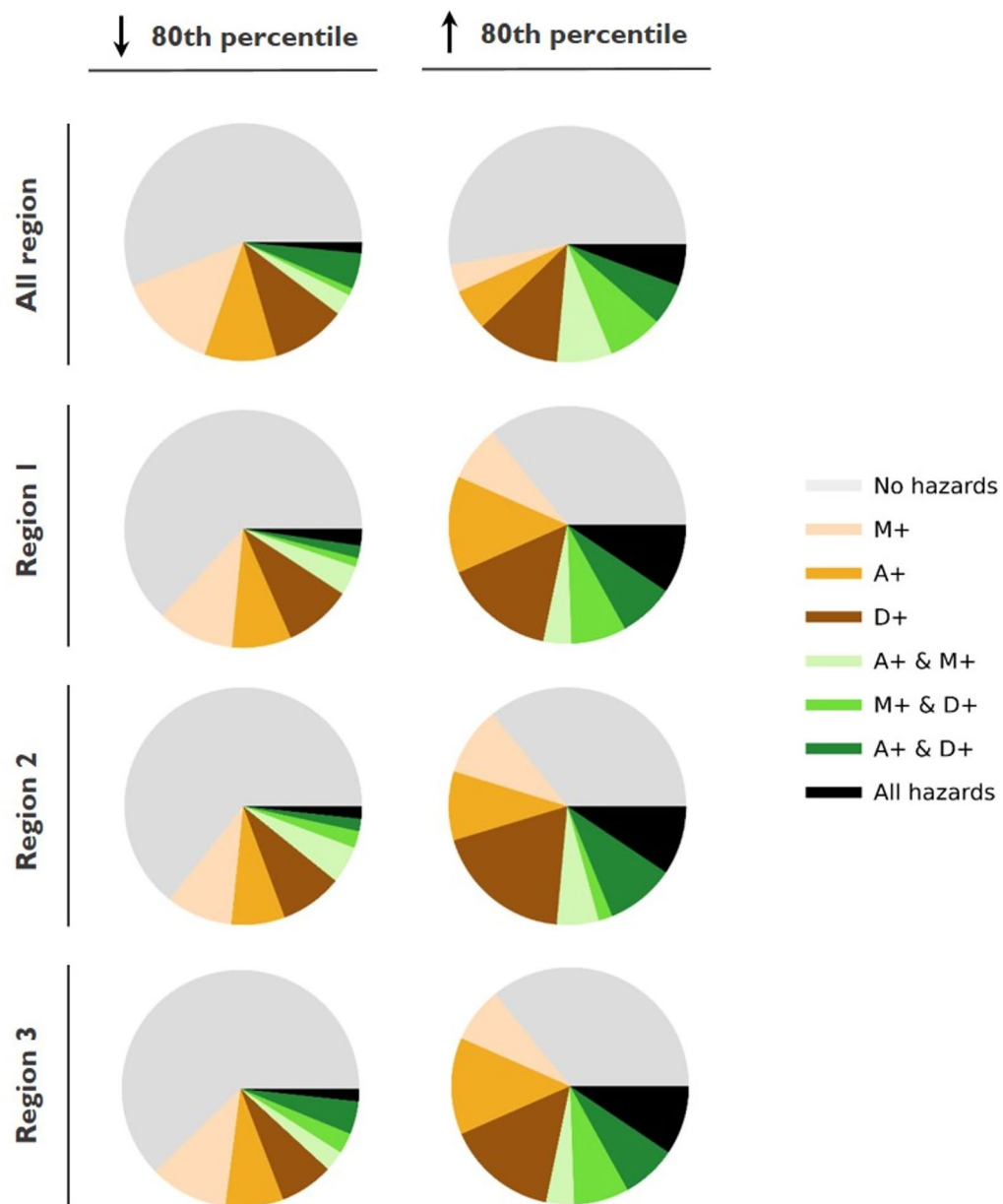


Figure 9. Single and compound climatic hazards and its association with wildfires. These charts show the portion of months, shown in Fig. 8, that are associated to each of type of hazard or combined hazards. This analysis only considers months where any burned area was registered. The categorization is distinguished by the different regions of study and the predefined threshold for burned areas (80th percentile).

than 25% of all months. The presence of all hazards together (A+, M+ and D+) is associated with 6% to 9% of the months in these cases.

Discussion

The temporal evolution of four key characteristics of heatwaves is analysed: frequency, mean duration, mean intensity and cumulative intensity (ICI), which all show a notable upward trend in both the atmosphere and ocean over the whole period of study. AHWs consistently record higher levels of yearly mean intensities. The high variability in AHWs mean intensities and longer MHWs mean durations is attributed to the heat capacity, persistence, and propagation timescales of oceanic processes, which are much greater than those for the atmosphere⁵⁷. The fluctuations in ICI levels within both the atmosphere and the ocean often show synchronized patterns of escalation and reduction. This observation underscores the indication of a possible robust association between both variables, suggesting a noteworthy correlation in the occurrence of atmospheric and marine extreme hot events.

When assessing drought conditions, the period 2000–2022 reveals a higher incidence of years marked by drier conditions when compared to the preceding century, which experienced a higher occurrence of wetter years. This indicates a notable shift in drought conditions between both periods. The percentage of area under the occurrence of moderate and severe drought conditions show an increasing tendency over the whole period of study.

The identified rising trends in these extreme climatic events align with previous studies that have historically analyzed atmospheric and marine heatwaves^{4,12}, as well as drought characteristics^{95,96}, and emphasize the need for increasing awareness of these phenomena, particularly considering projections indicating a future escalation in their occurrence^{14,41,95–97}.

The negative correlations between T2m and P values have intensified in the most recent period, particularly in the full region and region 2. This result agrees with the previous works conducted by^{40,96} that attribute this correlation to the amplification of the land–atmosphere feedback in the presence of warmer conditions. Elevated temperatures and increased radiative forcing lead to greater evaporation rates, which might result in earlier-season soil dehydration. This, in turn, could lead to decreased evaporative cooling effects during the summer period. The strong positive correlation between T2m over land and SST over the adjacent regions observed in both periods highlights the close connection between air temperatures over land and sea surface temperatures in the adjacent oceans, as already suggested by^{60,61} underscoring the significance of considering both air and ocean temperatures when studying regional climate dynamics and climate extremes. Correlations between SST and P values resulted in non-significant negative values. The understanding of the complex interactions between SSTs and precipitation patterns still offers ample opportunities for exploration. References^{59,98} have directed their focus on the co-occurrence of extreme sea temperature and drought conditions, over eastern South America and California coast, respectively. However, the relationship between marine heatwaves and land-occurring hazards is still a challenge, particularly because of the non-existence of a spatial overlap of the studied variables. Thus, approaching this type of problem constitutes a challenge.

The extent of burned areas in Europe has exhibited significant variability throughout the twenty-first century. According to our results, the years 2003, 2005, 2017 and 2022 stand out as having the most extensive burned area in the analysed areas of Western Europe. In the eastern European region, the burned area was particularly high in 2007, 2012, 2017 and 2021.

Dry and hot conditions can be significant contributors to severe fire years across various European regions. Different European regions may show varying patterns, but most of the years of severe fire coverage were associated with reduced precipitation and elevated air temperatures during the summer season. This finding aligns with conclusions drawn in earlier research studies on the same topic^{10,11,25,33,34}.

In this study, we also integrated sea surface temperatures into our analysis of compound extremes. This variable was found to be closely associated with the occurrence of other extremes known to significantly impact the occurrence of wildfires. Furthermore, it was concluded that, in the Iberian Peninsula, the Mediterranean Sea is distinguished by consistently recording elevated SST (and marine ICI) values when compared to the Atlantic Ocean, suggesting a possible closer association between extreme climate events in the Iberian Peninsula and the Mediterranean water temperatures.

The long-term interplay between marine heatwave, atmospheric heatwave and drought conditions and their association with burned pixels is assessed on an annual scale. In several cases, years with extreme marine heatwave conditions corresponded with the occurrence of stronger atmospheric heatwave and dry conditions over burned regions. Conversely, years with lower marine heatwave intensity are mostly associated with less dry and/or warm conditions over burned areas. A negative trend between atmospheric heatwave and drought indices was found for all regions under investigation.

Short-term occurrences of single and compound extreme climatic conditions over burned pixels are also explored. Over all areas of study, months with total burned area below the 80th percentile threshold show to be considerably associated with stronger warm events over the ocean, although 60% of the months did not record any associated extreme hazard. This significant percentage can be attributed to the utilization of a particularly high threshold applied to heatwaves and droughts in our analysis, since we only focus on the 20% of historical most extreme cases. Additionally, fire activity can be influenced by a variety of factors beyond extreme fire weather, including vegetation conditions and human factors affecting ignition and fire spread⁹⁹. The occurrence of wildfires can also be closely linked to pre-fire season conditions, as investigated by³⁴. The authors explore the interplay between antecedent drought conditions leading up to the simultaneous occurrence of extreme heat indicators in the exceptional fire season that affected southern continental Greece in the summer of 2007. This accentuates the importance of accounting for time-lags between climatic hazards, unravelling the complex synergies among antecedent conditions and concurrent seasonal hazards in forthcoming research on this topic.

Months in which the total accumulated burned area surpasses the 80th percentile are mostly associated to extreme climatic conditions across the analysed sub-regions. The most prevalent hazard across all months shows to be the presence of stronger dry conditions. The occurrence of compound events becomes more evident, while non-extreme climatic factors become less pronounced compared to the previous case. This suggests that the simultaneous occurrence of very hot and dry extremes potentially amplify the occurrence of large wildfires.

Conclusions

As climate change progresses, the escalation of extreme climatic hazards, such as heatwaves and droughts, has become increasingly prevalent. The compounding effects of these hazards may be amplified when they occur simultaneously or in a cascading sequence, significantly contributing to wildfire occurrence. This work aims to improve the comprehension of the linkage between atmospheric and marine heatwaves, droughts, and the occurrence of rural fires in the Mediterranean region throughout the past decades. The investigation of the interconnection between land-based atmospheric conditions and sea surface temperatures uncovers new insights in a domain that has not been extensively investigated before.

In the long-term assessment, the interplay between marine heatwaves, atmospheric heatwaves, and drought conditions on an annual scale reveals a noteworthy pattern. Years marked by more extreme marine heatwave conditions often coincide with intensified atmospheric heatwave and dry conditions over burned regions.

Short-term assessments of single and compound extreme climatic conditions over burned pixels provide additional insights. Marine hot conditions emerge as the most common hazard for months in which burned areas remain below the 80th percentile threshold, while strong dry events prevail for months in which burned areas surpass this threshold. Months characterized by such extensive fires are predominantly associated to extreme climatic conditions (atmospheric heatwaves, marine heatwaves, dry conditions) across the analysed regions. The combined occurrence of these events also becomes more evident, while non-extreme climatic factors are less pronounced.

The linkage between atmospheric and oceanic conditions further underscores the need to consider both factors when studying regional climate dynamics and compound extremes, suggesting potential for further in-depth investigation. While our study has examined the co-occurrence of marine heatwaves and land-based hazards, and their possible association with the occurrence of rural fires, there remains a critical need for future analysis to unravel the underlying mechanisms driving these concurrent occurrences, considering both atmospheric and oceanic factors, utilizing additional data (e.g., heat fluxes, wind, vertical velocity) and advanced approaches to provide a more comprehensive understanding of their interplay. Disclosing the coupling mechanisms related to these extreme warm and dry events and understanding their respective driving roles, especially in the context of phenomena like fire incidence, would offer valuable insights for predictions and effective risk management. While the absence of spatial overlap between marine and land variables poses a challenge, it also opens opportunities to explore the role of atmospheric teleconnections and large-scale circulation patterns in connecting them. Consideration of timescales and potential lag effects would also be essential for clarifying the relationship between these geographically distinct components of the climate system.

There is an urgent need to explore the potential impacts of these compound episodes on wildfires. This analysis might be crucial for improving fire management and preparedness, and providing clear guidelines for the risk management of such a meteorological disaster. The findings of this work are not only relevant to the local context but also hold global significance, as the challenges posed by compound extreme events extend far beyond this region. In the Pantanal, compound drought-heatwave conditions in 2020 have led to the most catastrophic fire season over the last two decades, leading to significant environmental repercussions²⁶. The 2019–2020 Australian bushfire season and the 2020 California wildfires both underscore the role of prolonged hot and dry conditions in setting the stage for unprecedented fire activity^{51,52}. These examples of other globally recognized fire-prone regions reflect our observations in the Mediterranean, where climate-driven compound events have similarly increased wildfire risk, and have also been marked by significant marine heatwave episodes^{59,98,100}. This emphasizes the global importance of considering compound extreme events in fire management strategies, as climate change continues to drive an increase in the frequency and severity of extreme events globally while threatening the stability of ecosystems.

Data availability

Data relevant to the analysis can be downloaded from the Copernicus database for the ERA5 reanalysis datasets, available at <https://cds.climate.copernicus.eu/cdsapp#!/search?type=dataset> and from The Land Processes Distributed Active Archive Center, accessible at <https://lpdaac.usgs.gov/products/mcd64a1v006/>.

Code availability

The code used in this study is available upon request to the authors.

Received: 28 December 2023; Accepted: 7 August 2024

Published online: 20 August 2024

References

1. Pörtner, H.-O., et al. (2022). IPCC 2022: Climate change 2022: Impacts, adaptation and vulnerability: Working group II contribution to the sixth assessment report of the intergovernmental panel on climate change.
2. Hobday, A. J. et al. A hierarchical approach to defining marine heatwaves. *Prog. Oceanogr.* **141**, 227–238 (2016).
3. Oliver, E. C. et al. Longer and more frequent marine heatwaves over the past century. *Nat. Commun.* **9**(1), 1–12 (2018).
4. Perkins-Kirkpatrick, S. & Lewis, S. Increasing trends in regional heat-waves. *Nat. Commun.* **11**(1), 3357 (2020).

5. Pastor, F. & Khodayar, S. Marine heat waves: Characterizing a major climate impact in the Mediterranean. *Sci. Total Environ.* **861**, 160621 (2023).
6. Ibrahim, O., Mohamed, B. & Nagy, H. Spatial variability and trends of marine heat waves in the eastern mediterranean sea over 39 years. *J. Mar. Sci. Eng.* **9**(6), 643 (2021).
7. McMichael, A. J. & Lindgren, E. Climate change: Present and future risks to health, and necessary responses. *J. Internal Med.* **270**(5), 401–413 (2011).
8. Robine, J.-M. *et al.* Death toll exceeded 70,000 in Europe during the summer of 2003. *Comptes Rendus Biol.* **331**(2), 171–178 (2008).
9. Parente, J., Pereira, M., Amraoui, M. & Fischer, E. M. Heat waves in Portugal: Current regime, changes in future climate and impacts on extreme wildfires. *Sci. Total Environ.* **631**, 534–549 (2018).
10. Ruffault, J. *et al.* Increased likelihood of heat-induced large wildfires in the mediterranean basin. *Sci. Rep.* **10**(1), 13790 (2020).
11. García-Herrera, R., Díaz, J., Trigo, R. M., Luterbacher, J. & Fischer, E. M. A review of the European summer heat wave of 2003. *Crit. Rev. Environ. Sci. Technol.* **40**(4), 267–306 (2010).
12. Simon, A. *et al.* Hot and cold marine extreme events in the mediterranean over the period 1982–2021. *Front. Mar. Sci.* **9**, 892201 (2022).
13. Ruthrof, K. X. *et al.* Subcontinental heat wave triggers terrestrial and marine, multi-taxa responses. *Sci. Rep.* **8**(1), 13094 (2018).
14. Oliver, E. C. *et al.* Projected marine heatwaves in the 21st century and the potential for ecological impact. *Front. Mar. Sci.* **6**, 734 (2019).
15. Vicente-Serrano, S. M., McVicar, T. R., Miralles, D. G., Yang, Y. & Tomas- Burguera, M. Unraveling the influence of atmospheric evaporative demand on drought and its response to climate change. *Wiley Interdiscip. Rev. Clim. Change* **11**(2), e632 (2020).
16. Salvador, C. *et al.* Effects of drought on mortality in macro urban areas of Brazil between 2000 and 2019. *GeoHealth* **6**(3), e2021GH000534 (2022).
17. Gouveia, C., Trigo, R. M., Beguería, S. & Vicente-Serrano, S. M. Drought impacts on vegetation activity in the mediterranean region: An assessment using remote sensing data and multi-scale drought indicators. *Glob. Planet. Change* **151**, 15–27 (2017).
18. Guion, A. *et al.* Droughts and heatwaves in the western mediterranean: Impact on vegetation and wildfires using the coupled wrf-orchidee regional model (regipsl). *Clim. Dynam.* **58**(9–10), 2881–2903 (2022).
19. Gouveia, C. M., Silva, M., & Russo, A. (2024). The severity of dry and hot climate extremes and their related impacts on vegetation in Madagascar. *Iscience.* **27**(1), 108658.
20. Bento, V. A., Russo, A., Vieira, I. & Gouveia, C. M. Identification of forest vulnerability to droughts in the Iberian Peninsula. *Theoret. Appl. Climatol.* **152**(1–2), 559–579 (2023).
21. Ermitão, T., Gouveia, C. M., Bastos, A. & Russo, A. C. Interactions between hot and dry fuel conditions and vegetation dynamics in the 2017 fire season in Portugal. *Environ. Res. Lett.* **17**(9), 095009 (2022).
22. Madadgar, S., AghaKouchak, A., Farahmand, A. & Davis, S. J. Probabilistic estimates of drought impacts on agricultural production. *Geophys. Res. Lett.* **44**(15), 7799–7807 (2017).
23. Páscoa, P. *et al.* Drought trends in the Iberian Peninsula over the last 112 years. *Adv. Meteorol.* **2017**, 4653126 (2017).
24. Ribeiro, A. F. S., Russo, A., Gouveia, C. M., Páscoa, P., and Zscheischler, J. Risk of crop failure due to compound dry and hot extremes estimated with nested copulas, *Biogeosciences*, **17**, 4815–4830.
25. Turco, M. *et al.* On the key role of droughts in the dynamics of summer fires in mediterranean Europe. *Sci. Rep.* **7**(1), 81 (2017).
26. Libonati, R. *et al.* Assessing the role of compound drought and heatwave events on unprecedented 2020 wildfires in the Pantanal. *Environ. Res. Lett.* **17**(1), 015005 (2022).
27. Stahl, K. *et al.* Impacts of European drought events: Insights from an international database of text-based reports. *Nat. Hazards Earth Syst. Sci.* **16**(3), 801–819 (2016).
28. Després, J., Adamovic, M. Seasonal impacts of climate change on electricity production—JRC PESETA IV project Task 4, EUR 29980 EN, Publications Office of the European Union, Luxembourg, 2020, ISBN 978-92-76-13095-6
29. Tramblay, Y. *et al.* Challenges for drought assessment in the Mediterranean region under future climate scenarios. *Earth-Sci. Rev.* **210**, 103348 (2020).
30. Giorgi, F. & Lionello, P. Climate change projections for the mediterranean region. *Glob. Planet. Change* **63**(2–3), 90–104 (2008).
31. Tuel, A. & Eltahir, E. A. Why is the mediterranean a climate change hot spot?. *J. Clim.* **33**(14), 5829–5843 (2020).
32. Ganteaume, A., Barbero, R., Jappiot, M. & Maille, E. Understanding future changes to fires in southern Europe and their impacts on the wildland-urban interface. *J. Safety Sci. Resilience* **2**(1), 20–29 (2021).
33. Turco, M. *et al.* Climate drivers of the 2017 devastating fires in Portugal. *Sci. Rep.* **9**(1), 13886 (2019).
34. Gouveia, C. M. *et al.* The outstanding synergy between drought, heatwaves and fuel on the 2007 southern Greece exceptional fire season. *Agric. Forest Meteorol.* **218**, 135–145 (2016).
35. Ramos, A. M., Russo, A., DaCamara, C. C., Nunes, S., Sousa, P., Soares, P., Lima, M. M., Hurduc, A., & Trigo, R. M. (2023). The compound event that triggered the destructive fires of October 2017 in Portugal. *Iscience.* **26**(3).
36. Zscheischler, J. *et al.* Future climate risk from compound events. *Nat. Clim. Change* **8**(6), 469–477 (2018).
37. Bevacqua, E. *et al.* Guidelines for studying diverse types of compound weather and climate events. *Earth's Future* **9**(11), e2021EF002340 (2021).
38. Sutanto, S. J., Vitolo, C., Di Napoli, C., D'Andrea, M. & Van Lanen, H. A. Heatwaves, droughts, and fires: Exploring compound and cascading dry hazards at the pan-European scale. *Environ. Int.* **134**, 105276 (2020).
39. Hao, Z. *et al.* Compound droughts and hot extremes: Characteristics, drivers, changes, and impacts. *Earth-Sci. Rev.* **235**, 104241 (2022).
40. Zscheischler, J. & Seneviratne, S. I. Dependence of drivers affects risks associated with compound events. *Sci. Adv.* **3**(6), e1700263 (2017).
41. Seneviratne, S. I., Zhang, X., Adnan, M., Badi, W., Dereczynski, C., Di Luca, A., Ghosh, S., Iskander, I., Kossin, J., Lewis, S., et al. (2021). Weather and climate extreme events in a changing climate (chapter 11).
42. Hao, Z., Hao, F., Singh, V. P. & Zhang, X. Changes in the severity of compound drought and hot extremes over global land areas. *Environ. Res. Lett.* **13**(12), 124022 (2018).
43. Ridder, N. N., Ukkola, A. M., Pitman, A. J. & Perkins-Kirkpatrick, S. E. Increased occurrence of high impact compound events under climate change. *NPJ Clim. Atmos. Sci.* **5**(1), 3 (2022).
44. Ban, J., Lu, K., Wang, Q. & Li, T. Climate change will amplify the inequitable exposure to compound heatwave and ozone pollution. *One Earth* **5**(6), 677–686 (2022).
45. Burger, E. A., Terhaar, J. & Frölicher, T. L. Compound marine heatwaves and ocean acidity extremes. *Nat. Commun.* **13**(1), 4722 (2022).
46. Le Grix, N., Zscheischler, J., Laufkötter, C., Rousseaux, C. S., and Frölicher, T. L. Compound high-temperature and low-chlorophyll extremes in the ocean over the satellite period. *Biogeosciences*, **18**, 2119–2137
47. Jang, M. T. G. *et al.* Increased chlorophyll-a concentration in Barra Bonita reservoir during extreme drought periods. *Sci. Total Environ.* **843**, 157106 (2022).
48. Hamdeno, M., Nagy, H., Ibrahim, O. & Mohamed, B. Responses of satellite chlorophyll-a to the extreme sea surface temperatures over the Arabian and Omani Gulf. *Remote Sensing* **14**(18), 4653 (2022).

49. Plecha, S. M. & Soares, P. M. Global marine heatwave events using the new cmip6 multi-model ensemble: From shortcomings in present climate to future projections. *Environ. Res. Lett.* **15**(12), 124058 (2020).
50. Kwiatkowski, L. *et al.* Twenty-first century ocean warming, acidification, deoxygenation, and upper-ocean nutrient and primary production decline from CMIP6 model projections. *Biogeosciences* **17**(13), 3439–3470 (2020).
51. Abram, N. J. *et al.* Connections of climate change and variability to large and extreme forest fires in southeast Australia. *Commun. Earth Environ.* **2**(1), 8 (2021).
52. Varga, K. *et al.* Megafires in a warming world: What wildfire risk factors led to California's largest recorded wildfire. *Fire* **5**(1), 16 (2022).
53. Belhadj-Khedher, C., El-Melki, T. & Moullot, F. Saharan hot and dry sirocco winds drive extreme fire events in mediterranean tunisia (north Africa). *Atmosphere* **11**(6), 590 (2020).
54. Trigo, R. M. *et al.* Atmospheric conditions associated with the exceptional fire season of 2003 in Portugal. *Int. J. Climatol.* **26**(13), 1741–1757 (2006).
55. Fischer, E. M. & Knutti, R. Anthropogenic contribution to global occurrence of heavy-precipitation and high-temperature extremes. *Nat. Clim. Change* **5**(6), 560–564 (2015).
56. Amengual, A. *et al.* Projections of heat waves with high impact on human health in Europe. *Glob. Planet. Change* **119**, 71–84 (2014).
57. Plecha, S. M., Soares, P. M., Silva-Fernandes, S. M. & Cabos, W. On the uncertainty of future projections of marine heatwave events in the north Atlantic ocean. *Clim. Dynam.* **56**(7–8), 2027–2056 (2021).
58. Holbrook, N. J. *et al.* Keeping pace with marine heatwaves. *Nat. Rev. Earth Environ.* **1**(9), 482–493 (2020).
59. Rodrigues, R. R., Taschetto, A. S., Sen Gupta, A. & Foltz, G. R. Common cause for severe droughts in south America and marine heatwaves in the south Atlantic. *Nat. Geosci.* **12**(8), 620–626 (2019).
60. Aboulkhai, H., Mohamed, B., Morsy, M. & Nagy, H. Co-occurrence of atmospheric and oceanic heatwaves in the eastern mediterranean over the last four decades. *Remote Sensing* **15**(7), 1841 (2023).
61. Pathmeswaran, C., Sen Gupta, A., Perkins-Kirkpatrick, S. E. & Hart, M. A. Exploring potential links between co-occurring coastal terrestrial and marine heatwaves in Australia. *Front. Clim.* **4**, 37 (2022).
62. Hu, L. A global assessment of coastal marine heatwaves and their relation with coastal urban thermal changes. *Geophys. Res. Lett.* **48**(9), e2021GL093260 (2021).
63. Olita, A. *et al.* Effects of the 2003 European heatwave on the central mediterranean sea: Surface fluxes and the dynamical response. *Ocean Sci.* **3**(2), 273–289 (2007).
64. Feudale, L. & Shukla, J. Role of mediterranean sst in enhancing the European heat wave of summer 2003. *Geophys. Res. Lett.* **34**(3), L03811 (2007).
65. Sparnocchia, S., Schiano, M., Picco, P., Bozzano, R. & Cappelletti, A. The anomalous warming of summer 2003 in the surface layer of the central ligurian sea (western mediterranean). *Annales Geophysicae* **24**(2), 443–452 (2006).
66. Galizia, L. F., Curt, T., Barbero, R. & Rodrigues, M. Understanding fire regimes in Europe. *Int. J. Wildland Fire* **31**(1), 56–66 (2021).
67. Turco, M. *et al.* Decreasing fires in mediterranean Europe. *PLoS One* **11**(3), e0150663 (2016).
68. Copernicus Climate Change Service, Climate Data Store, (2019): Land cover classification gridded maps from 1992 to present derived from satellite observation. *Copernicus Climate Change Service (C3S) Climate Data Store (CDS)*. <https://doi.org/10.24381/cds.006f2c9a> (Accessed on 22-02-2023)
69. Hersbach, H., Bell, B., Berrisford, P., Bivat, G., Horanyi, A., Munoz Sabater, J., Nicolas, J., Peubey, C., Radu, R., Rozum, I., *et al.* (2023). Era5 hourly data on single levels from 1940 to present, *copernicus climate change service (c3s) climate data store (cds)*. (Accessed on 14-09-2022)
70. Hersbach, H. *et al.* The era5 global reanalysis. *Quart. J. R. Meteorol. Society* **146**(730), 1999–2049 (2020).
71. Giglio, L., Justice, C., Boschetti, L., Roy, D. (2015). MCD64A1 MODIS/Terra+Aqua Burned Area Monthly L3 Global 500m SIN Grid V006. *NASA EOSDIS Land Processes Distributed Active Archive Center*. Accessed 2023-02-15 from 10.5067/MODIS/MCD64A1.006
72. Giglio, L., Boschetti, L., Roy, D. P., Humber, M. L. & Justice, C. O. The collection 6 modis burned area mapping algorithm and product. *Remote Sensing Environ.* **217**, 72–85 (2018).
73. AppEEARS Team. (2023). Application for Extracting and Exploring Analysis Ready Samples (AppEEARS). Ver. X.X. NASA EOSDIS Land Processes Distributed Active Archive Center (LP DAAC), USGS/Earth Resources Observation and Science (EROS) Center, Sioux Falls, South Dakota, USA. Accessed 02, 01, 2023. <https://appears.earthdatacloud.nasa.gov/>
74. Robusto, C. C. The cosine-haversine formula. *Am. Math. Monthly* **64**(1), 38–40 (1957).
75. Russo, A. *et al.* Assessing the role of drought events on wildfires in the Iberian peninsula. *Agric. Forest Meteorol.* **237**, 50–59 (2017).
76. Rodrigues, M., Peña-Angulo, D., Russo, A., Zuñiga-Antón, M. & Cardil, A. Do climate teleconnections modulate wildfire-prone conditions over the Iberian Peninsula?. *Environ. Res. Lett.* **16**(4), 044050 (2021).
77. Bekar, I. & Taşlıoğlu, C. Modelling the drivers of natural fire activity: The bias created by cropland fires. *Int. J. Wildland Fire* **26**(10), 845–851 (2017).
78. Perkins, S. E. A review on the scientific understanding of heatwaves—Their measurement, driving mechanisms, and changes at the global scale. *Atmos. Res.* **164**, 242–267 (2015).
79. Perkins, S. E. & Alexander, L. V. On the measurement of heat waves. *J. Clim.* **26**(13), 4500–4517 (2013).
80. Zhang, X. *et al.* Indices for monitoring changes in extremes based on daily temperature and precipitation data. *Wiley Interdiscip. Rev. Clim. Change* **2**(6), 851–870 (2011).
81. World Meteorological Organization. (2018). Guide to climatological practices [[Accessed 10-2023]]. <https://library.wmo.int/idurl/4/60113>
82. Golubeva, E., Kraineva, M., Platov, G., Iakshina, D. & Tarkhanova, M. Marine heatwaves in Siberian Arctic Seas and adjacent region. *Remote Sensing* **13**(21), 4436 (2021).
83. Russo, A., Gouveia, C., Dutra, E., Soares, P. & Trigo, R. M. The synergy between drought and extremely hot summers in the mediterranean. *Environ. Res. Lett.* **14**(1), 014011 (2019).
84. Vogel, J., Paton, E., Aich, V. & Bronstert, A. Increasing compound warm spells and droughts in the mediterranean basin. *Weather Clim. Extremes* **32**, 100312 (2021).
85. McKee, T. B., Doesken, N. J., Kleist, J., *et al.* (1993). The relationship of drought frequency and duration to time scales. *Proceedings of the 8th Conference on Applied Climatology*, **17** (22), 179–183.
86. World Meteorological Organization. (2012). Standardized Precipitation Index User Guide [[Accessed 10-2023]]. <https://library.wmo.int/records/item/39629-standardized-precipitation-index-user-guide>
87. Vicente-Serrano, S. M., Beguería, S. & López-Moreno, J. I. A multiscalar drought index sensitive to global warming: The standardized precipitation evapotranspiration index. *J. Clim.* **23**(7), 1696–1718 (2010).
88. Hargreaves, G. H. Defining and using reference evapotranspiration. *J. Irrigation Drainage Eng.* **120**(6), 1132–1139 (1994).
89. Spinoni, J., Naumann, G. & Vogt, J. V. Pan-European seasonal trends and recent changes of drought frequency and severity. *Glob. Planet. Change* **148**, 113–130 (2017).

90. Vicente-Serrano, S. M. *et al.* Reference evapotranspiration variability and trends in Spain, 1961–2011. *Glob. Planet. Change* **121**, 26–40 (2014).
91. Agnew, C. Using the SPI to identify drought. *Drought Netw. News* **1994–2001**, 1 (2000).
92. Bevacqua, E., Zappa, G., Lehner, F. & Zscheischler, J. Precipitation trends determine future occurrences of compound hot–dry events. *Nat. Clim. Change* **12**(4), 350–355 (2022).
93. Pereira, M. G., Trigo, R. M., da Camara, C. C., Pereira, J. M. & Leite, S. M. Synoptic patterns associated with large summer forest fires in Portugal. *Agric. Forest Meteorol.* **129**(1–2), 11–25 (2005).
94. Turco, M. *et al.* Exacerbated fires in Mediterranean Europe due to anthropogenic warming projected with non-stationary climate–fire models. *Nat. Commun.* **9**(1), 3821 (2018).
95. Spinoni, J., Naumann, G., Vogt, J., & Barbosa, P. (2016). Meteorological droughts in Europe: Events and impacts–past trends and future projections.
96. Vicente-Serrano, S. M. *et al.* Evidence of increasing drought severity caused by temperature rise in southern Europe. *Environ. Res. Lett.* **9**(4), 044001 (2014).
97. Lhotka, O., Kyselý, J. & Farda, A. Climate change scenarios of heat waves in central Europe and their uncertainties. *Theor. Appl. Climatol.* **131**(3–4), 1043–1054 (2018).
98. Shi, H. *et al.* Co-occurrence of California drought and northeast pacific marine heatwaves under climate change. *Geophys. Res. Lett.* **48**(17), e2021GL092765 (2021).
99. Jones, M. *et al.* Global and regional trends and drivers of fire under climate change. *Rev. Geophys.* **60**(3), e2020RG000726 (2022).
100. Oliver, E. C. *et al.* The unprecedented 2015/16 Tasman Sea marine heatwave. *Nat. Commun.* **8**(1), 16101 (2017).

Acknowledgements

This work was supported by the European Union’s Horizon 2020 research project FirEURisk, with the Grant Agreement no. 101003890 and by national funds through FCT I.P./MCTES (Fundação para a Ciência e a Tecnologia) (PIDAAC) - UIDB/50019/2020 (<https://doi.org/10.54499/UIDB/50019/2020>), UIDP/50019/2020 (<https://doi.org/10.54499/UIDP/50019/2020>) and LA/P/0068/2020 (<https://doi.org/10.54499/LA/P/0068/2020>) and by <https://doi.org/https://doi.org/10.54499/2022.09185.PTDC> (project DHEFEUS). AR acknowledges FCT for 2022.01167.CEECIND (Complex).

Author contributions

The study was conceptualised by all authors. R.S. collected data, performed all the calculations and was responsible for the data curation and analysis. R.S. also designed all the figures and wrote the manuscript. All the authors contributed to the conception of the work, analyzed the results, wrote, reviewed and approved the final version of the manuscript.

Additional information

Supplementary Information The online version contains supplementary material available at <https://doi.org/10.1038/s41598-024-69691-y>.

Correspondence and requests for materials should be addressed to R.S.

Reprints and permissions information is available at www.nature.com/reprints.

Publisher’s note Springer Nature remains neutral with regard to jurisdictional claims in published maps and institutional affiliations.

Open Access This article is licensed under a Creative Commons Attribution-NonCommercial-NoDerivatives 4.0 International License, which permits any non-commercial use, sharing, distribution and reproduction in any medium or format, as long as you give appropriate credit to the original author(s) and the source, provide a link to the Creative Commons licence, and indicate if you modified the licensed material. You do not have permission under this licence to share adapted material derived from this article or parts of it. The images or other third party material in this article are included in the article’s Creative Commons licence, unless indicated otherwise in a credit line to the material. If material is not included in the article’s Creative Commons licence and your intended use is not permitted by statutory regulation or exceeds the permitted use, you will need to obtain permission directly from the copyright holder. To view a copy of this licence, visit <http://creativecommons.org/licenses/by-nc-nd/4.0/>.

© The Author(s) 2024